JBIC Journal of Biological Inorganic Chemistry (2025) 30:329–344
https://doi.org/10.1007/s00775-025-02120-1

MINI REVIEW

Magnetic interactions between metal sites in complex enzymes

Biplab K. Maiti[1] · Isabel Moura[2] · José J. G. Moura[2]

Received: 25 February 2025 / Accepted: 15 July 2025 / Published online: 24 July 2025

Abstract

Magnetic interactions between iron–sulfur (Fe/S) clusters and transition metal centers such as nickel, molybdenum, and copper play a central role in the function of key metalloenzymes. These interactions, which arise from electronic coupling, spin exchange, and spatial arrangement, directly influence redox behavior and catalytic efficiency. This review highlights three distinct complex enzymes—[NiFe] hydrogenases, mononuclear molybdenum-containing xanthine oxidase (XO) family, and [NiFe] and [MoCu] carbon monoxide dehydrogenases (CODHs)—as paradigms for understanding (Fe/S)-metal center interactions. In [NiFe] hydrogenases, (Fe/S) clusters serve as electron relays that magnetically interact with the catalytic [NiFe] active site. In XO-type enzymes, a mononuclear Mo center is functionally and magnetically coupled to nearby Fe/S clusters, modulating substrate reduction and electron transfer. Similarly, in CODHs, both [NiFe]—and [MoCu]-dependent variants exhibit strong magnetic communication between metal active sites and surrounding Fe/S clusters, crucial for CO_2/CO interconversion. Advanced spectroscopic approaches, particularly electron paramagnetic resonance (EPR) and related techniques, combined with theoretical modelling, have provided deep insights into the electronic structures and dynamic interactions within these metalloenzymes. Understanding these magnetic interactions not only sheds light on fundamental electron-transfer and enzymatic mechanisms but also guides the design of bioinspired catalysts and energy-conversion technologies.

Graphical abstract

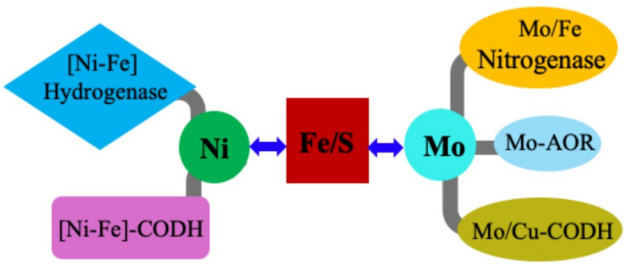

Keywords Magnetic interactions · Electron transfer · Iron–sulfur centers · [NiFe] Hydrogenase · Aldehyde oxidoreductase · CO dehydrogenase

Abbreviations

AOR	Aldehyde oxidoreductase
CODH	Carbon monoxide dehydrogenase
Ch	*Carboxydothermus hydrogenoformans*
Da	*Desulfovibrio alaskensis*
Dd	*Desulfivibrio desulfuricans* ATCC2774
Dg	*Desulfovibrio gigas*
DgAOR	*Desulfovibrio gigas* Aldehyde oxidoreductase
DgHase	*Desulfovibrio gigas* Hydrogenase
DvM	*Desulfovibrio vulgaris* Myasaki

✉ Biplab K. Maiti
biplabmaiti@clujammu.ac.in

✉ José J. G. Moura
jose.moura@fct.unl.pt

[1] School of Sciences, Department of Chemistry, Cluster University of Jammu, Jammu 180001, India

[2] LAQV, NOVA School of Sciences and Technology, Campus de Caparica, 2829-516 Caparica, Portugal

DvMHase	*Desulfovibrio vulgaris* Myasaki hydrogenase
ENDOR	Electron-nuclear double resonance
EPR	Electron Paramagnetic Resonance
ET	Electron transfer
FAD	Flavin adenine dinucleotide
Fd	Ferredoxin
Fe/S	Iron-sulfur cluster
Feu	Unique iron
Hase	Hydrogenase
LPMO	Lytic polysaccharide monooxygenases
MB	Mossbauer spectroscopy
Moco	Molybdenum cofactor
MPT	Molybdopterin
Mt	*Moorella thermoacetic*
Ma	*Methanococcus aeolicus*
NHE	Normal hydrogen Electrode
PDB	Protein Data Bank
PCET	Proton-coupled electron transfer
Rr	*Rhodospirillum rubrum*
XO	Xanthine oxidase

Introduction

Magnetic interactions between iron–sulfur (Fe/S) clusters and other active metal sites, such as nickel, molybdenum and copper, are crucial for the catalytic activity and structural stability of many metalloenzymes including nitrogenases, hydrogenases, carbon monoxide dehydrogenase (CODH) and mononuclear molybdenum enzymes, which play essential roles in key biological processes such as nitrogen fixation, hydrogen metabolism, carbon processing, and sulfur assimilation [1–10].

The interplay between Fe/S centers and active-site metals is mediated by electronic coupling, spin exchange, and structural proximity, which influence the redox properties and reactivity of these enzymes [1–17]. This review focuses on bacterial [NiFe] hydrogenases (highlighting nickel's interaction with Fe/S centers) [7, 13, 16], and molybdenum enzymes, ranging from mononuclear forms to more complex systems and examining molybdenum interactions with other metal centers: specific examples include the xanthine oxidase enzyme family (such as aldehyde oxidoreductase) [8, 17], and CODH ([MoCu] and also [NiFe] variants) [11, 12].

Advances in understanding these magnetic interactions are driven by spectroscopic techniques such as electron paramagnetic resonance (EPR) and related techniques, and computational modelling. Insights gained from these studies enhance our knowledge of metalloenzyme function, guiding the design of biomimetic catalysts and promoting applications in sustainable energy and biotechnology. These findings underscore the intricate role of magnetic interactions in fine-tuning enzymatic performance, bridging the gap between bioinorganic chemistry and functional enzyme engineering.

[NiFe] Hydrogenase, a special class of hydrogen-metabolizing enzymes

Nature possesses a class of enzymes, notably hydrogenases (Hases), which reversibly cleave molecular hydrogen into electrons and protons: $H_2 \leftrightarrow 2e^- + 2H^+$ [7]. Hydrogenases are generally classified as iron-sulfur-containing proteins, with iron atoms arranged in different cluster configurations [7]. At least, three different types are now recognized within this bacterial group: [FeFe] hydrogenases, contains several [4Fe-4S] clusters and an active site considered an atypical Fe/S cluster termed the "H-cluster" [7, 18, 19]; [NiFe] hydrogenases with one nickel and iron-sulfur centers generally arranged as one [3Fe4S] and two [4Fe4S] clusters [7, 20, 21] (subgroup [NiFeSe] hydrogenases with iron-sulfur centers and equimolecular amounts of nickel and selenium (Ni bound to a selenium cysteine)) found in bacteria and archaea [7, 22, 23], and the third class of hydrogenases, [Fe]-hydrogenase contains a mononuclear iron center with no Fe/S cluster found only in some *hydrogenotrophic methanogenic* archaea [24]. The structures of metal active sites of various hydrogenases are depicted in Fig. 1. Among them, [NiFe] Hases are the main focus of this article.

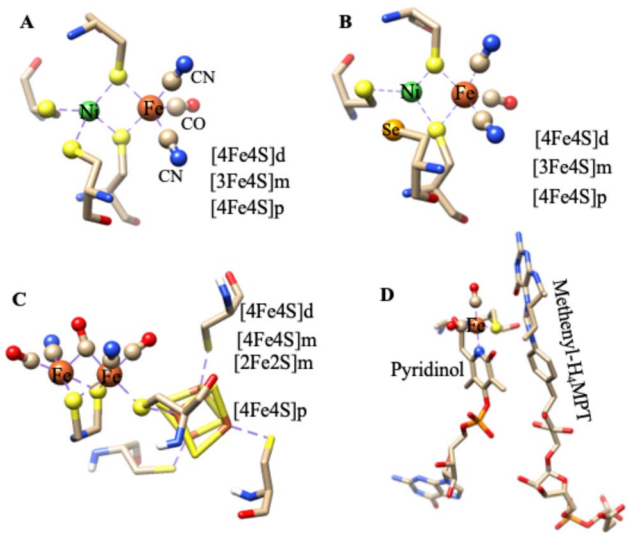

Fig. 1 3D structures of active sites of three types of hydrogenases (Hases): **A** [NiFe]-Hase from *Desulfovibrio gigas* (PDB: 1YQ9), **B** [NiFeSe]-Hase from *Desulfomicrobium baculatum* (PDB:1CC1) **C** [FeFe]-Hase from *Clostridium pasteurianum* (PDB: 4XDC), and **D** Fe-Hase from *Methanococcus aeolicus* (PDB:6HAV). [4Fe4S]d: distal iron-sulfur, [3Fe4S]m: mediator iron-sulfur, and [4Fe4S]p: proximal iron-sulfur cluster

[NiFe] hydrogenases are subdivided into two subgroups: (a) O_2-sensitive [NiFe] hydrogenases that are inhibited under oxic conditions, and (b) O_2-tolerant [NiFe] hydrogenases that can sustain activity under oxic conditions [7, 21, 25, 26]. The 3D structural features of both O_2-sensitive and O_2-tolerant [NiFe] hydrogenases are shown in Fig. 2. Both have similar active site structures, but the main difference is found in the proximal iron-sulfur cluster, [4Fe3S]-6Cys cluster in O_2-tolerant and classical [4Fe4S] cluster in O_2-sensitive-hydrogenase. The binuclear active site, [NiFe], is attached to the protein chain by four cysteine residues. Two cysteines bridged the metal centers (Fe and Ni), and the other two cysteine residues were terminally coordinated to the nickel site. In addition, biologically unusual CO and CN^- ligands are coordinated to Fe-ion in active sites and make them fascinating examples of 'organometallic' cofactors [7, 21, 25, 26].

The [NiFe] Hydrogenases isolated from sulfate-reducing bacteria, particularly *Desulfovibrio* (*D.*) species, have served as model systems. In particular, extensive work has been performed on the hydrogenase isolated from *Desulfovibrio gigas,* a prototype of the [NiFe] hydrogenases [27–36], and the 3D structure was first reported, in 1995, by Volbeda and co-workers [21, 25]. *D. gigas* hydrogenase has a molecular mass of 89 kDa (subunits: 26 kDa and 63 kDa) and contains four redox centers: one nickel–iron center, one [3Fe4S], and two [4Fe-4S] clusters (Fig. 2A) [21, 25].

EPR and Mössbauer (MB) spectroscopy have been the primary tools for studying the metal center composition of the enzyme, revealing the presence of four non-interacting centers: one [NiFe] center (where the Ni was assigned to an unusual trivalent oxidation state), one [3Fe4S] cluster (EPR-active), and two [4Fe4S] clusters (EPR-silent) [7, 16, 37, 38]. Intermediate redox species generated upon hydrogen interaction indicate that nickel is redox-active, cycling between trivalent and divalent oxidation states. These oxidation states are associated with redox-linked activation steps essential for full enzymatic activity. Three "faces" of the [NiFe] center have been identified in the isolated state as well as in the catalytic cycle by EPR: Ni-A (inactive), Ni-B (inactive-ready), and Ni-C (hydride bound), all of them in the formal + III state. Ni-C interacts with a proximal [4Fe4S] cluster. In addition, the oxidation state of nickel is formally + II in the case of Ni-Si_a ("nickel-silent-active") [7, 16, 21, 23, 37–45], and Ni(I) in Ni-C light reacted (see below) (Fig. 3). Further redox state variations have been determined via the IR absorbance of the CO/CN^- ligands [46, 47]. The shifting of vibrational bands of CO/CN^- ligands between variable redox states arises from the alteration in electron density at their active sites. Indeed, the stretching vibration bands of νCO in Ni-A, Ni-B, Ni-SI, and Ni-C states for [NiFe] hydrogenases from *D. gigas* are observed at 1947 cm^{-1}, 1946 cm^{-1}, 1934 cm^{-1}, and 1952 cm^{-1}, respectively, suggesting different redox states in the entire catalytic cycle [46, 47].

The isolated aerobic enzyme (resting)

In the "aerobically as-isolated" enzyme, the nickel center is EPR-active, exhibiting two rhombic signals: a strong signal (Ni-signal A, Ni-A) with g-values at 2.31, 2.26, and 2.02, and a weaker signal (Ni-signal B, Ni–B) at 2.33, 2.16, and

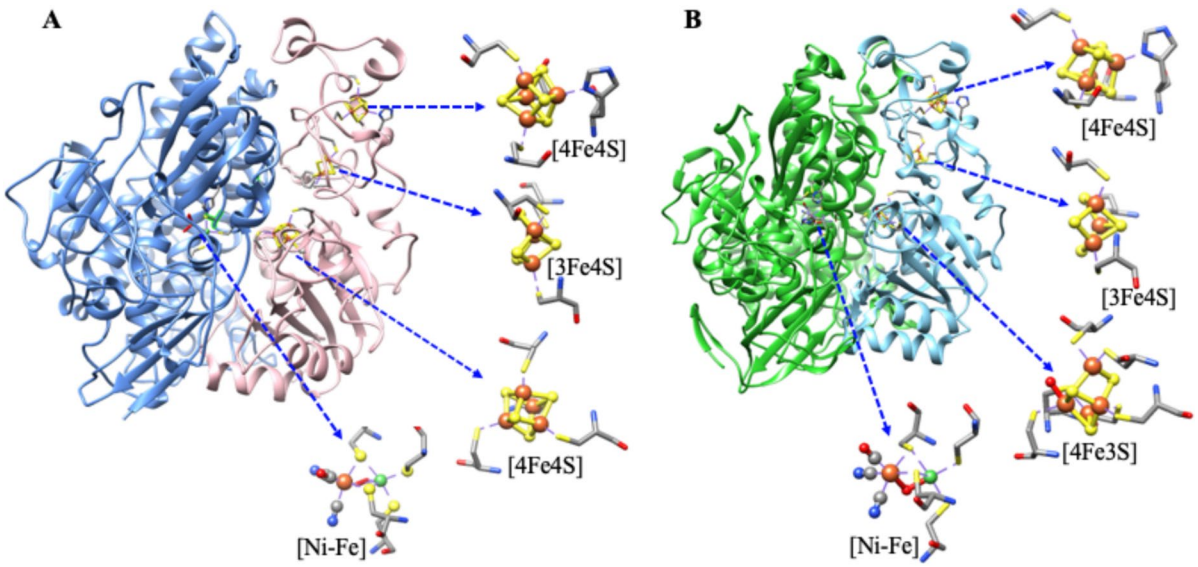

Fig. 2 **A** O_2- sensitive) [NiFe] hydrogenases from *Desulfovibrio gigas* (PDB: 1YQ9), and **B** O_2-tolerant [NiFe] hydrogenases from *Ralstonia eutropha* (PDB: 4IUB). Highlighted the active site as well as iron-sulfur clusters

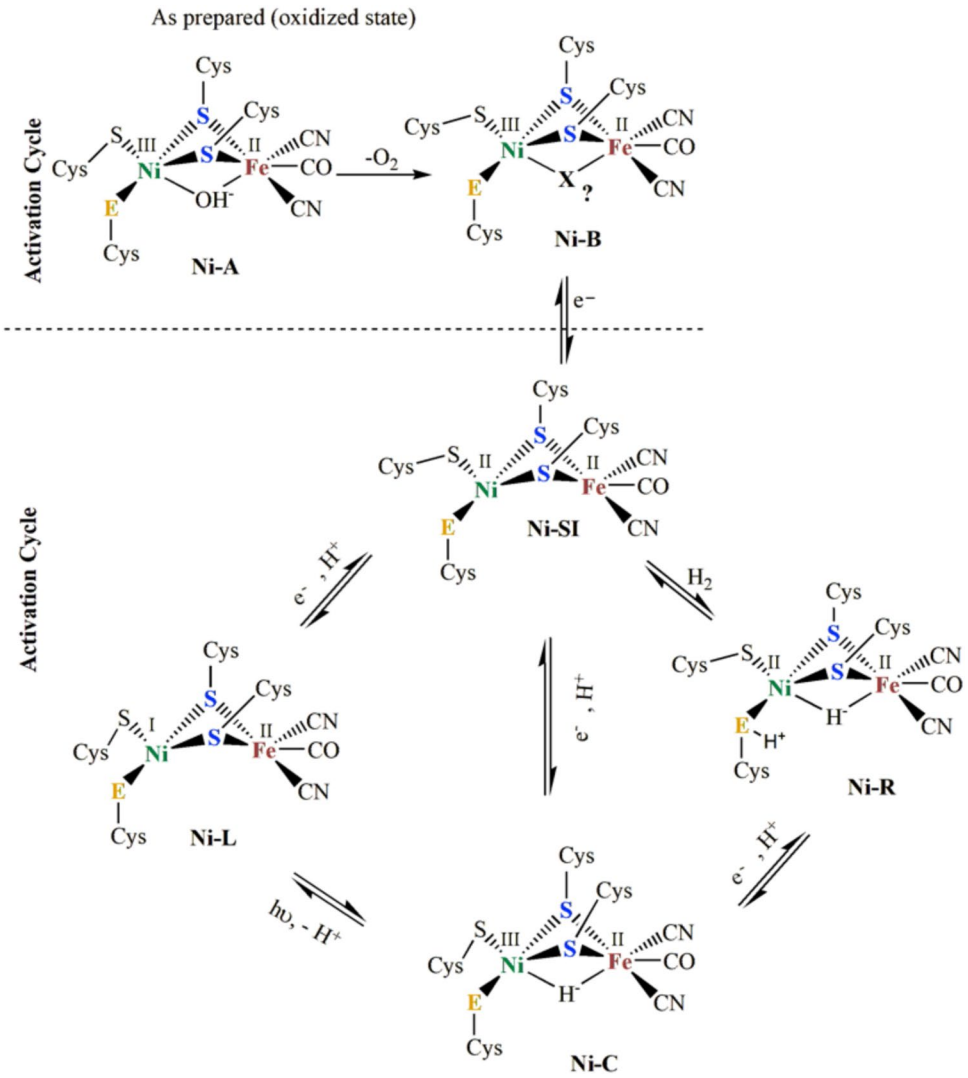

Fig. 3 Different Oxidation states of [NiFe] Hydrogenase are involved in the activation and catalytic cycle. Adapted from [46]

2.02 [7, 16, 48, 49] (Fig. 4). Both signals remain observable up to 100 K without broadening. Ni-A and Ni-B states are key states in the initiation of the enzyme catalytic cycle, particularly in oxygen tolerance and reactivation processes. These states are oxidized forms of the active site and are distinguished based on their reactivity and spectroscopic signatures. Ni-A slowly reactivates under reducing conditions (termed the "unready" oxidized state), while Ni-B rapidly reactivates under reducing conditions (termed the "ready" oxidized state). More oxygen-tolerant hydrogenases tend to accumulate Ni-B rather than Ni-A [7, 16, 46–51].

Their relative intensities vary with protein preparation, and Ni-B can be enhanced by anaerobic redox cycling, suggesting to contain different oxygenated bound species. Isotopic substitution with (^{61}Ni (I = 3/2) causes line broadening at $g_1 = 2.31$ and resolved hyperfine structures at $g_2 = 2.23$ ($^{61}A_2 = 1.5$ mT) and $g_3 = 2.02$ ($^{61}A_3 = 2.7$ mT), confirming that the paramagnetic nickel is at the origin of these signals [51]. This species is attributed to a low-spin Ni(III) center in a tetragonally distorted octahedral S = 1/2 system, with an unpaired electron in a dz^2 orbital [32].

Combined EPR and Mössbauer spectroscopy definitively established an oxidized [3Fe4S] center (S = 1/2) (similar to the one isolated in *D. gigas* Ferredoxin II (FdII), a prototype of a [3Fe4S] cluster [52], with hyperfine broadening in EPR signals of ^{57}Fe-enriched samples [13, 30]. The 4.2 K Mössbauer spectra of native and ^{57}Fe-enriched samples revealed an intense quadrupole doublet, indicating two oxidized EPR-silent (S = 0) $[4Fe4S]^{+2}$ clusters [30, 33]. These findings confirm that this hydrogenase contains four distinct redox centers: one nickel center, one [3Fe4S] cluster, and two [4Fe4S] clusters, which do not interact in their as-prepared state.

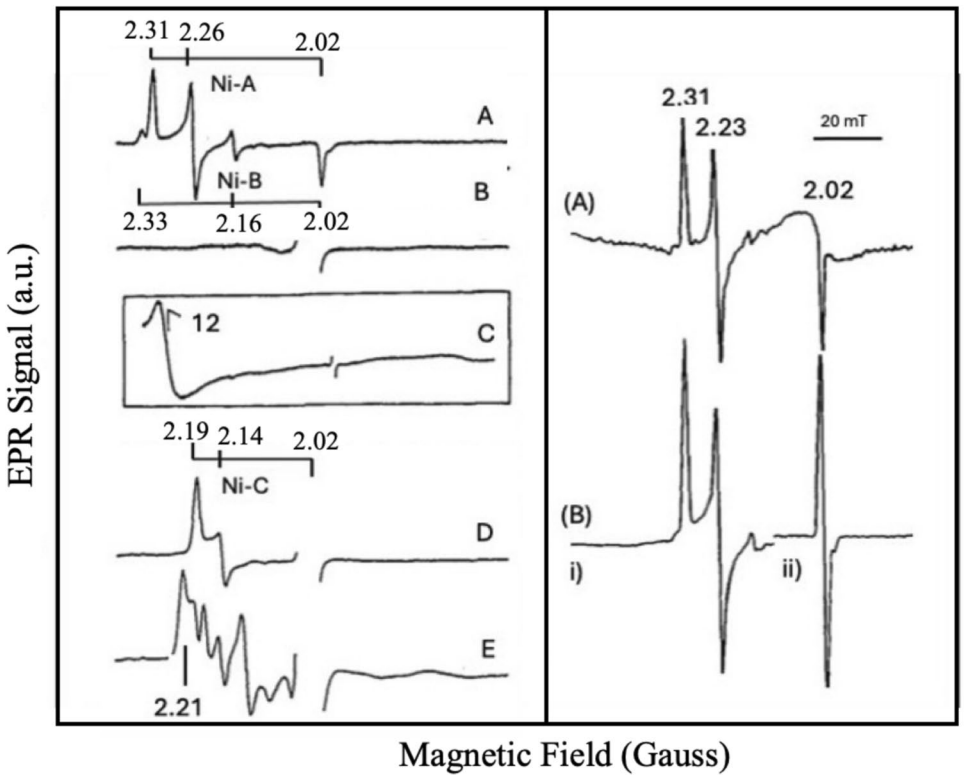

Fig. 4 Representative spectra of *Desulfovibrio gigas* Hase (oxidized and H_2 reacted). Left panel—**A** Native sample as isolated (oxidized state). Ni-A and Ni–B signals are observed at 77 K. (**B**) The so-called "EPR silent", at 20 K. **C** The "g = 12" signal, "EPR silent" state as in **B**, but now observed in a wide field range at 4.2 K. **D** Ni-C signal at 20 K. **E** Same as **D**, but observed at 4.2 K. Right panel—Native sample as isolated. **A** Sample containing Ni-A signal as major species at 77 K. **B** Some as **A** but at 10 K. (i) Ni(III) features, (ii) g, 2.0 spectral region dominated by the [3Fe-4S]ox cluster. In addition, a schematic representation highlights the g-values associated with Ni-A, Ni-B and Ni-C. More details in the text. Adapted from [32, 51]

Substrate-reacted enzyme – active state—magnetic interactions

Structural reorganization of the Ni and [4Fe4S] centers upon reaction with H_2

(i) Ni signals Upon hydrogen interaction, the g = 2.02 signal from the $[3Fe4S]^{+1}$ center disappears first [30, 34] (mid-point redox potential −70 mV (NHE), pH-independent), followed by the loss of Ni-signals A and B (Ni-A has a mid-point potential −220 mV (NHE) and pH-dependent at 60 mV/pH unit), leading to a silent Ni(II) state [30–34], but concomitantly, a broad low-field signal (crossover at g≈12) emerges, resembling the "g = 12" signal attributed to a S = 2 spin state, similar to *D. gigas* ferredoxin II, which contains a single [3Fe4S] cluster [53]. (Fig. 4).

Mössbauer studies confirmed that, in fully reduced samples, the [3Fe4S] cluster remains reduced (S = 2) and does not convert to a [4Fe4S] cluster [33], indicating its presence in a catalytically active state. At this stage, the two [4Fe4S] centers are reduced to the + 1 state and remain spectroscopically distinct. After activation under hydrogen gas (or redox poising) restores a paramagnetic state of the nickel center, producing a transient rhombic EPR signal (Ni-C) with $g_1 = 2.19$, $g_2 = 2.14$, and $g_3 = 2.02$ appears but disappears with prolonged hydrogen exposure or excess sodium dithionite [31–33]. Isotopic substitution confirmed its assignment to Ni(III) ($^{61}A_3 = 2.0$ mT) [54]. The Ni-C state is one of the most critical and well-studied intermediates in the catalytic cycle of [NiFe] hydrogenases and represents a key paramagnetic, reduced state involved in hydrogen activation. It is an active state in hydrogen catalysis and can be reduced further to Ni-R (fully reduced, Ni(II)), which releases hydrogen. It can be oxidized back to Ni-SI (inactive Ni(II)) under certain conditions. The Ni-C state forms when the hydrogen heterologous cleaves, a proton (H^+) going to a nearby base and a hydride (H^-) binding between Ni and Fe [7, 16, 21, 55]. The Ni-L site in light-activated [NiFe] hydrogenases is a crucial intermediate in the enzyme's catalytic cycle, particularly influenced by light [7, 16, 21, 56]. Ni-L (Light-sensitive state) is a reduced, paramagnetic (Ni(I)) state of the Ni–Fe active site. It is part of the catalytic cycle, occurring when the active Ni-SI state receives an electron. Ni-L is characterized by a low-spin Ni(I) center, stabilized by the Fe-S cluster. Ni-L is highly light-sensitive, and exposure to light can accelerate its conversion to the Ni-SI state (Ni(II)) (see Fig. 3). This photoconversion is due to energy absorption, which facilitates electron transfer and structural rearrangements at the active site. EPR (Electron Paramagnetic Resonance) spectroscopy identifies Ni-L as a Ni(I) species with distinct signals [7, 16, 21, 56, 57].

(ii) The nature of the ligands between Ni and Fe in different redox states of [NiFe] Hydrogenases. The Ni-A (S = 1/2) is associated with the as-isolated (unready) form and features a nonprotein ligand (X) bridging the two met-

als. Ni-A and Ni-B states have been proposed to have a bridging hydroxide (OH^-) ligand between Ni and Fe, having in Ni-B more flexible coordination environment (see Fig. 3). This ligand is proposed to be oxygenic (O^{2-} or OH^-) in *Dg*.

Hase and an inorganic sulfide in *DvM*Hase. To determine its nature in *Dg*Hase, 35 GHz CW ^{17}O ENDOR measurements were conducted with Ni-A containing major species exchanged into $H_2{}^{17}O$, the active Ni-C state (formed by H_2-reduction of Ni-A in $H_2{}^{17}O$), and Ni-A regenerated by reoxidizing Ni-C in $H_2{}^{17}O$ [39, 50, 58, 59].

In native Ni-A, the bridging ligand does not exchange with solvent. However, after a Ni-A → Ni-C → Ni-A cycle, an ^{17}O label appears at the active site, as confirmed by ENDOR. The substantial isotropic component ($a_{iso}(^{17}O) \approx$ 11 MHz) confirms that the solvent-derived ^{17}O ligates Ni, identifying X in Ni-A as an oxygenic species. This aligns with prior EPR results suggesting the same for Ni-B [60].

The small ^{57}Fe hyperfine coupling observed in Ni-A ($A(^{57}Fe) \sim 0.9$ MHz) persists in Ni-C ($A(^{57}Fe) \sim 0.8$ MHz), but the ^{17}O signal vanishes upon reduction to Ni-C and reappears upon reoxidation to Ni-A. Analysis of the electronic structure suggests that the oxygenic bridge in Ni-A(B) is lost in Ni-C and reforms from solvent upon reoxidation. This implies that Ni-C formation opens Ni/Fe coordination sites, potentially playing a key role in enzyme activity [50, 58–60].

(iii) Ni site and magnetic interactions. At low temperatures (< 10 K), another complex g = 2.21 EPR signal emerges at redox levels around Ni-C formation [32, 61]. The observation of this signal requires high microwave power, indicating a fast-relaxing species. A heterolytic hydrogen cleavage mechanism has been proposed in bacterial hydrogenases [59]. Ni-C was initially attributed to a nickel-hydride species [31, 32], but the relaxation behavior of the g = 2.21 signal suggests spin–spin interactions rather than a simple paramagnet (see Fig. 4). It was further interpreted as a split Ni-C signal due to interaction with a $[4Fe4S]^{+1}$ cluster [61].

Supporting this assignment was the study of redox states of the enzyme prepared, with the [4Fe4S] clusters either diamagnetic or paramagnetic. In the paramagnetic state, magnetic coupling between metal centers induces a complex low-temperature EPR spectrum, a split Ni-C signal, and increased Ni center relaxation rates. Simulations of the split Ni-C signal at X-, Q-, and S-band frequencies, using a point dipole model for dipolar and exchange interactions, confirm that only one $[4Fe4S]^{+1}$ cluster is significantly coupled to the Ni site [63]. This provided a detailed description of their relative arrangement, by spin–spin and spin–lattice relaxation times were measured in both redox states using power saturation, pulsed EPR at low temperatures, and EPR line broadening studies at higher temperatures [63].

Mononuclear molybdenum enzymes of the xanthine oxidase family

Aldehyde oxidoreductases (AORs) from various *Desulfovibrio* species—*D. gigas*, *D. alaskensis*, *D. aminophilus*, and *D. desulfuricans* are homologous enzymes within the molybdenum hydroxylase family. These enzymes catalyze the hydroxylation of aldehydes to carboxylic acids [8, 64–68]. As members of the xanthine oxidase (XO) enzyme family, these molybdoenzymes also contain two [2Fe2S] clusters, designated Fe/S I and Fe/S II, coordinated by distinct cysteine motifs (Fig. 5A and B). These clusters facilitate electron transfer from the substrate to an acceptor, such as an FAD moiety (as in XO) or an external electron-transferring protein [8, 61–68].

X-ray crystallography has shown that in *D. gigas* AOR (*Dg*AOR), the Fe/S I cluster is coordinated via a ferredoxin-type motif near the protein surface, while Fe/S II is ligated by an atypical cysteine motif and is in direct contact with the molybdopterin cofactor (Fig. 5B) [69, 70]. Relative distances between three cofactors in MOP, molybdopterin cytosine dinucleotide, [2Fe2S] center type I, and [2Fe2S] center type II are shown in Fig. 5C. The inter-connection between these redox cofactors is proposed as an electron-transfer pathway involving electron relay from one cofactor to another [69, 70]. The spectroscopic and crystallographic available data for *D. alaskensis*, *D. gigas,* and *D. desulfuricans* AORs support that both the spatial orientation and links among paramagnetic cofactors are conserved in this group of enzymes. The cluster spatial arrangement is illustrated in Fig. 5 from the gene sequence and crystal structure of the *Dd*AOR.

Figure 6 shows EPR spectra for *D. alaskensis* AOR under various conditions (oxidation states and temperatures), which probe magnetic interactions between the Mo site, nearby protons, and the Fe/S I cluster, as well as between Fe/S I and Fe/S II [68]. Two types of Mo(V)-associated EPR signals were identified: slow-type that develops after prolonged dithionite reduction, exhibiting nearly axial features with hyperfine splitting from a single proton (I = 1/2), confirmed using deuterium exchanged samples (Fig. 6-panel B, C) and rapid-type observed after benzaldehyde reduction, resembling a Michaelis complex analogue, also with proton hyperfine interactions (Fig. 6-panel A), simulation included for deuterated and non-deuterated samples [68].

Additionally, spectroscopic detected splittings suggest super-exchange coupling between the Mo site and adjacent Fe/S clusters. Low-temperature (< 70 K) EPR spectra reveal two [2Fe2S] clusters: Fe/S I, with narrower linewidths visible at 50 K, and Fe/S II, with broader signals at 20 K. Redox poised samples demonstrate

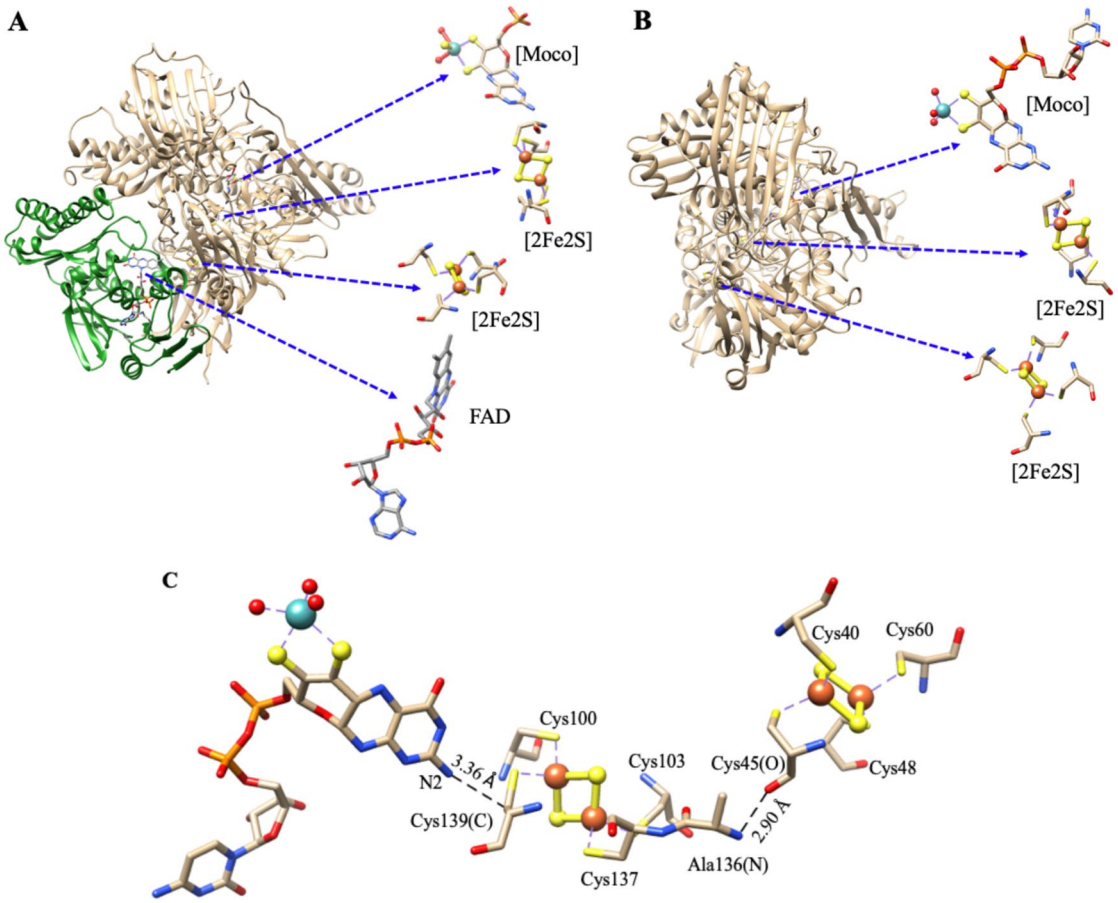

Fig. 5 3D structures of Xanthine oxidase (PDB: 1FIQ, bovine milk) (**A**) and Aldehyde oxidoreductase (PDB: 1VLB, *D. gigas*) (**B**). XO contains four redox centers: a molybdenum cofactor (MoCo, molybdopterin cytosine dinucleotide), two [2Fe2S] centers, and an FAD moiety. AOR shares strong structural similarities with XO but lacks the FAD-binding domain (green) found in XO. **C** The relative arrangement and interaction of three cofactors in AOR, molybdopterin cytosine dinucleotide, [2Fe2S] center type I, and [2Fe2S] center type II are shown by the X-ray crystal structure of AOR, and show a possible electron-transfer chain between three cofactors. Mo is shown as a cyan sphere, Fe as larger red spheres, S in yellow, and O in small red. Adapted from [69, 70]

temperature-dependent magnetic and super-exchange interactions between Mo(V) and the proximal Fe/S I center, evidenced by isotropic splittings and enhanced relaxation [68, 71, 72]. Dipolar interactions dominate between Fe/S I and Fe/S II (anisotropic splitting) (see Fig. 6-panels B and C). It is observed within this AOR class that the Fe/S I signal is fully split when the Fe/S II is fully sharpened. This fact, together with a similar spin concentration value for the two cofactors (detected in samples reduced with sodium dithionite at − 450 mV), indicates that reduction of Fe/S II produces magnetic coupling of the Fe/S I signal [68].

The magnitudes and type of splitting observed in *D. alaskensis* AOR are similar to those observed in the *D. gigas* [73] and *D. desulfuricans* [74] proteins, indicating that both the spatial orientation and links among paramagnetic cofactors are conserved in both AOR enzymes.

High-resolution structural data from *Dg*AOR enabled us to explore more deeply the magnetic interactions among its redox centers and to assign structurally the electronic pathways. Isotropic exchange coupling between the Mo center and the proximal Fe/S cluster was studied using native and polyalcohol-inhibited samples. EPR and QM/MM studies [17] modelled the Mo site as weakly coupled paramagnetic centers with distinct relaxation behavior [75–78].

The Fe/S I and Fe/S II centers could be distinguished by their g-values, temperature effects, redox potentials, and reduction rates [79, 80], in parallel to the results observed for *D. alaskensis* AOR. Their EPR signatures differ: Signal I (Fe/S I), less anisotropic, typical of ferredoxin-type signals ($g_{av} \sim 1.96$) and Signal II (Fe/S II) with broader spectral lines, higher g-values, and rapid relaxation properties attributed to low-lying excited states and double exchange interactions.

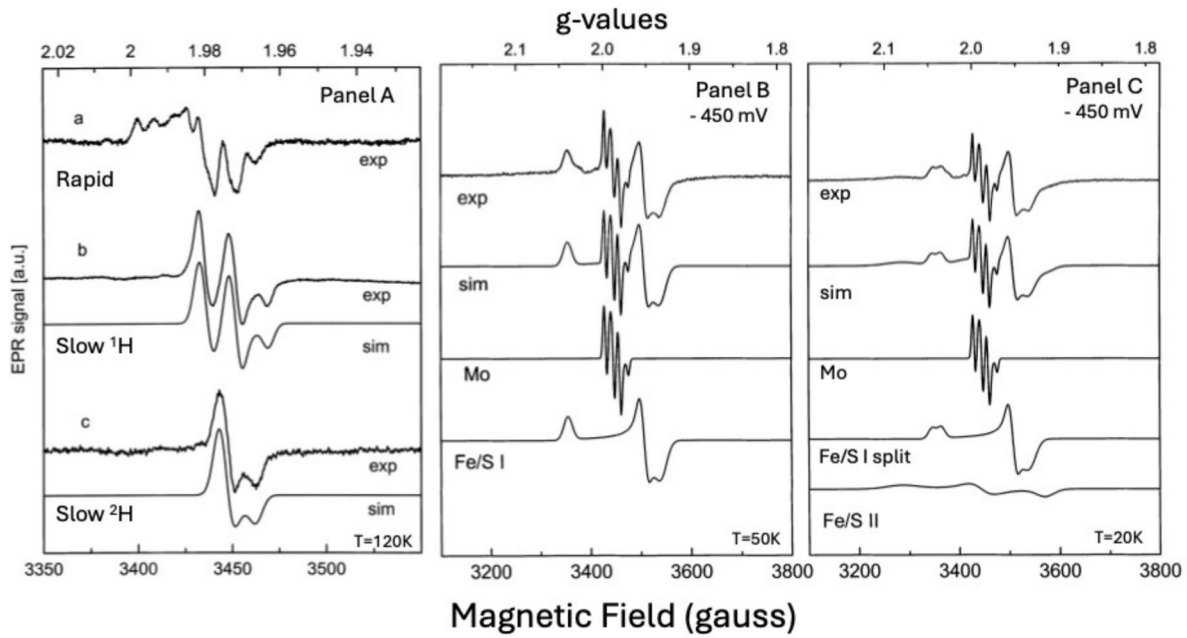

Fig. 6 EPR spectra of *D. alaskensis* AOR. **Panel A**—Mo(V) signals (a) Rapid-type signal obtained in as-isolated samples treated with benzaldehyde. (b) Slow-type signal obtained in samples after 10 min reaction with excess dithionite. (c) as (b) but in a deuterated sample. Experimental conditions: temperature, 120 K; microwave power, 2 mW; modulation amplitude, 4 G_{pp}; microwave frequency, 9.5 GHz. **Panel B**—samples at − 450 mV. Experimental conditions: temperature, 50 K; microwave power, 0.2 mW; modulation amplitude, 4 G_{pp}; microwave frequency, 9.5 GHz. **Panel C**—Experimental conditions: as in (**A**) except the temperature (20 K) and microwave power (0.06 mW). Simulations were performed as indicated in (ref). Adapted from [68]

Spectroscopic and structural assignment of the two $[2Fe2S]^{+1}$ clusters was aided by analyzing the Mo(V) EPR signal, as a probe [75, 81–85]. When all three metal centers are paramagnetic, spin–spin interactions cause spectral splitting at low temperatures. Modelling these based on the crystal structure allowed identification of the reducible [2Fe2S] clusters. Temperature-dependent behavior supports that Mo(V) couples magnetically with the cluster responsible for signal II—establishing this as the cluster nearest the Mo cofactor in both XO and *Dg*AOR [75, 81–85].

Combining crystallographic and EPR data enables a straightforward method to determine the relative positions of Fe/S clusters with respect to the Mo site. These spectroscopic insights are broadly applicable across the XO enzyme family, which consistently features two [2Fe2S] clusters and a Moco (molybdopterin cytosine dinucleotide or molybdopterin). In *Dg*AOR, the protein domain organization and cofactor environment define a buried, mechanistically distinctive catalytic site. The metal coordination geometries are well-resolved, and the proximity of redox centers (~ 12 Å) favors efficient intramolecular electron transfer during the catalytic cycle, mediated by the pterin cofactor [69, 70]. Spectroscopic evidence suggests that cofactor distances and orientations are preserved among all the homologs *Desulfovibrio sp.* AORs [69, 70].

From an evolutionary perspective, the 3D structures and cofactor arrangement in these enzymes are remarkable. The flavin domain serves as the terminal electron sink in XO and CO dehydrogenase ([MoCu]), see below [65, 86]. In *D. gigas* AOR, an external flavoprotein may fulfil this role [70]. A similar cofactor arrangement was recently proposed for CODH ([MoCu]), lacking its flavin domain [65, 70, 86]. Structurally, XO is a dimer of a single 300 kDa polypeptide with four cofactors [65]. CODH dehydrogenase is a dimer of three subunits (88 kDa molybdopterin, 30.2 kDa flavoprotein, 17.2 kDa Fe/S protein), sharing structural features with XO [62, 86]. AORs, in contrast, are dimers of shorter polypeptides lacking the flavin domain present in XO and CODH ([MoCu]). The Mo and Fe/S subunits of CODH ([MoCu]) are nearly superimposable on *D. gigas* AOR (70,86).

Carbon-monoxide dehydrogenase (CODH)

Carbon monoxide (CO) poisons many organisms, but particular microorganisms (both anaerobic and aerobic soil bacteria) have special metalloenzymes, namely carbon-monoxide dehydrogenase (CODH), which can use CO productively as the source of carbon and energy [5, 10, 11, 87, 88]. CODHs are classified into two classes based on their active sites and O_2 sensitivity [89]. The first class is

O_2-sensitive CODHs harbor heterometallic [NiFeS] cofactor, which catalyzes the reversible redox reaction (both directions), $CO + H_2O \leftrightarrow CO_2 + 2e^- + 2H^+$ [11, 87] with turnover frequency (TOF) of 40,000 s^{-1} for CO oxidation and 45 s^{-1} for CO_2 reduction [90]. The second class is non-O_2-sensitive CODHs harbouring heterometallic [MoCu] cofactor, which catalyzes the same redox reaction, in only one direction (oxidation direction) with a moderate TOF of 100 s^{-1} [86, 88].

[MoCu] CODH

The [MoCu] CODH belongs to the xanthine oxidase family. The crystal structure reveals that the protein is a dimer of a heterotrimer with 277 kDa [MoCu] containing iron-sulfur flavoprotein [86, 90–92]. Each heterotrimer is composed of an 88.7 kDa molybdoprotein (Large subunit (L)) containing the active site of CODH, a 30.2 kDa flavoprotein (Medium subunit (M)) containing FAD cofactor, and a 17.8 kDa iron-sulfur protein (small subunit (S)) containing two types of [2Fe2S] clusters (Fig. 7) [86, 90–92]. Its active site harbors an unprecedented heterobimetallic cluster composed of Cu and Mo; a bridging μ_2-S ligand connects these two metals. In the catalytic cycle, the fully oxidized state of Mo(VI) in the bimetallic center (Mo(VI)Cu(I)) of the [MoCu] CODH catalyzes the two-electron oxidation of CO to CO_2 with concomitant two-electron reduction of Mo(VI) to Mo(IV) (Mo(IV)Cu(I)). Therefore, during catalysis, Mo(VI) accepts electrons from the CO substrate to reduce to Mo(IV), and Cu(I) is capable of binding the CO substrate, but it remains same oxidation state due to a high degree of delocalization in the Mo-S-Cu unit [91, 93].

However, the detailed mechanism is still under debate [93–97]. During the re-oxidation of Mo^{IV} to Mo^{VI}, the Mo^{V} species may be generated from Mo(IV) by transferring one electron to a Fe/S cluster prior to completing the catalytic cycle. These cofactors establish an intramolecular electron transport that delivers the electrons generated through the oxidation of CO at the [$CuSMoO_2$] cluster to [2Fe2S] I, [2Fe2S] II, and finally to FAD, from where they are fed into a CO-insensitive respiratory chain to generate a membrane potential [98, 99]. The functional [MoCu] CODH is EPR silent, suggesting Cu(I) state, but inactive [MoCu] CODH shows a small Mo(V) signal like XOR, indicating loss of copper-sulfur bridge [99, 100]. In the catalytic cycle, the re-oxidation of Mo(IV) to Mo(VI) via Mo(V) by donating one electron to Fe–S cluster prior to complete the catalytic cycle. The Mo(V) shows a rhombic EPR signal with g_{xyz} (2.0010, 1.9604, 1.9549) and strong hyperfine coupling with Cu-nuclei (I = 3/2), A_{xyz} (117, 164, 132 MHz), indicating the high degree of electronic communication between Mo and Cu through the S-bridge [12, 86]. Interestingly, the EPR spectrum of active CODH enzyme disappears when it is treated with potassium cyanide and displays a new rhombic EPR signal at $g_{xyz} = 1.977$, 1.967, and 1.953, suggesting Cu affects the magnetic state of the Mo ion [86]. Moreover, Cu can be replaced by Ag in Mo/Cu-CODH under suitable conditions. When Cu(I) is replaced by Ag(I), the enzyme also shows Mo(V) EPR signal, with g_{xyz} (2.0043, 1.9595, 1.9540) and strong hyperfine coupling with Ag-nuclei (I = ½) with A_{xyz} (82, 79, 82 MHz) upon reduction with CO [5, 101]. The silver-substituted enzyme retains the catalytic activity of the native enzyme, with a slower rate constant compared to the native enzyme [101].

[NiFe] carbon monoxide dehydrogenases

The [NiFe] carbon monoxide dehydrogenases ([NiFe] CODH) catalyze the reversible interconversion of CO with

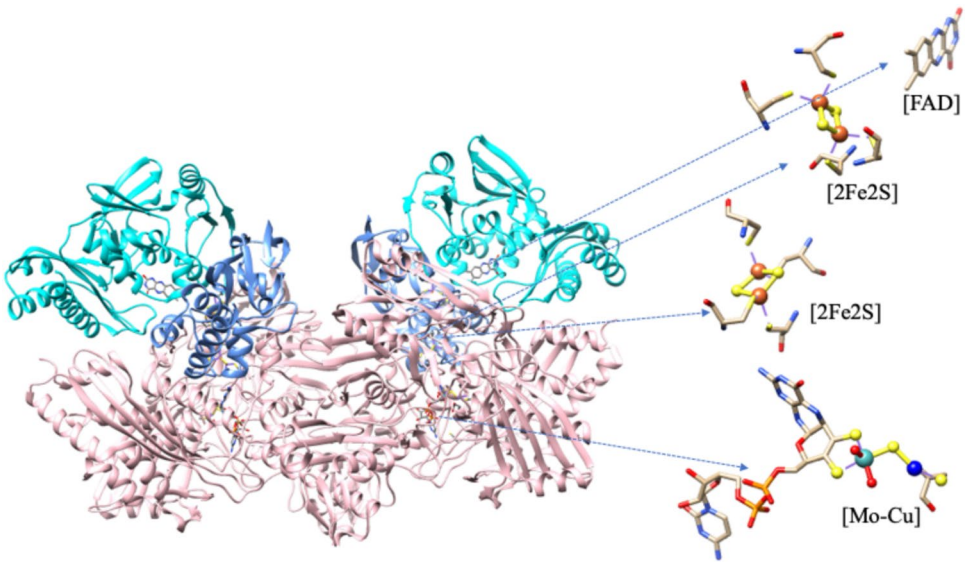

Fig. 7 Crystal structure of the dimer of trimer of aerobic [MoCu]-CODH from *O. carboxidovorans* (PDB: 1N5W): each trimer contains three subunits, including L-subunit; molybdo-protein (pink), S-subunit; Fe-S protein (blue) and M subunit; flavoprotein (cyan). Highlighted the [MoCu] active site, two [2Fe2S] clusters and FAD with distances among these redox components: Mo (cyan ball), Cu (blue ball), Fe (bigger red ball) S (yellow ball) and O (small red ball)

H_2O to CO_2 with $2H^+$ and $2e^-$ [6, 11, 102]. The 3D structures of [NiFe]-CODH from *Carboxydothermus hydrogenoformans* ($CODH_{Ch}$), *Moorella thermoacetica* ($CODH_{Mt}$), and *Rhodospirillum rubrum* ($CODH_{Rr}$) have been reported [103–107]. These organisms have the same protein structure, but have two different types of active site structures: [Ni4Fe5S] active center in $CODH_{Ch}$ and [Ni4Fe4S] active centre in $CODH_{Rr}$ and $CODH_{Mt}$.

The crystal structure of [NiFe]-CODH from *C. hydrogenoformans* is shown in Fig. 8. The [NiFe]-CODH is a large (molecular mass of 130 kDa) and complex homodimeric protein [104]. Each subunit harbors one conventional cubane-[4Fe4S] cluster (B-cluster), one asymmetrical [Ni4Fe5S] cluster (C-cluster), and an additional half part of the cubane [4Fe4S] cluster (D-cluster) at the interface of the dimer (Fig. 8A). Among them, the C-cluster is a catalytic centre where reversible reduction of CO_2 occurs [108, 109]. The C-cluster, [Ni4Fe5S], is an unusual structure where one Ni atom, three Fe atoms, and four inorganic S form a cuboidal-like [Ni3Fe4S] cluster, and one additional Fe atom (unique Fe or Feu) is extraneous to the [Ni3Fe4S] inserting at the Ni–S edge [103] and subsequent studies have demonstrated CO_2-bound C-cluster, [Ni4Fe4S(CO_2)] in which CO_2 is inserted between Ni and Feu (Fig. 8B) [110, 111].

The C-cluster has four oxidation states: a fully oxidized inactive state (C_{ox}), a one-electron reduced active state (C_{red1}), a two-electron reduced intermediate state (C_{int}), and a three-electron reduced active state (C_{red2}). C_{ox} and C_{int} both are EPR silent with spin state S = 0, whereas C_{red1} and C_{red2} both are EPR active, having spin states S = ½ and exhibiting EPR signals with $g_{1,2,3} = 2.01$, 1.81, and 1.65 and $g_{1,2,3} = 1.97$, 1.87, and 1.75, respectively [6, 102, 108, 112, 113]. Both states, C_{red1} and $C_{red2,}$ have similar EPR data, suggesting the unchanged electronic structure of [3Fe4S] fragment. The Ni K- and L-edge XAS studies described the low-spin EPR-silent Ni(II) for both C_{red1} and C_{red2} [114–116]. The absence of ^{61}Ni hyperfine coupling in the C_{red1} EPR signal suggests that electronically decoupled from the cluster and does not contribute to the spin-coupling mechanism [116]. The Mössbauer spectrum of C_{ox} shows a typical $[4Fe4S]^{2+}$ with no proof of Fe in Fe_u [102]. Mössbauer spectra of the C_{red1} state [112] describe high-spin Fe(II), Fe(III) oxidation states for [3Fe4S] fragment and high-spin Fe(II) oxidation state for Feu (unique Fe) [6, 102, 108].

The oxidation of CO involves $1e^-$ reductive activation of inactive C_{ox} to active C_{red1} at below potentials of − 100 mV, followed by $2e^-$ reduction to yield C_{red2} at below potential of − 500 mV, close to the potential of the CO/CO_2 redox couple [6, 102, 116].

The C_{red1}, C_{int}, and C_{red2} states are involved in the catalytic cycle. All proposed mechanisms generally presume that the CO_2-bound [Ni–Fe]-CODH structure represents a catalytic intermediate where the C atom of CO_2 is coordinated to Ni, one O atom of CO_2 is coordinated to Feu (Fig. 8B) [6, 102]. Based on the structure, the CO_2 binding to C_{red2} is thought to take place through a dissociative mechanism, yielding Ni-CO and Fe_u-OH, suggesting strong magnetic interactions between Ni and $Fe_{u.}$ This interaction disturbs the EPR g-values of C_{red1}, indicating the key role of spin

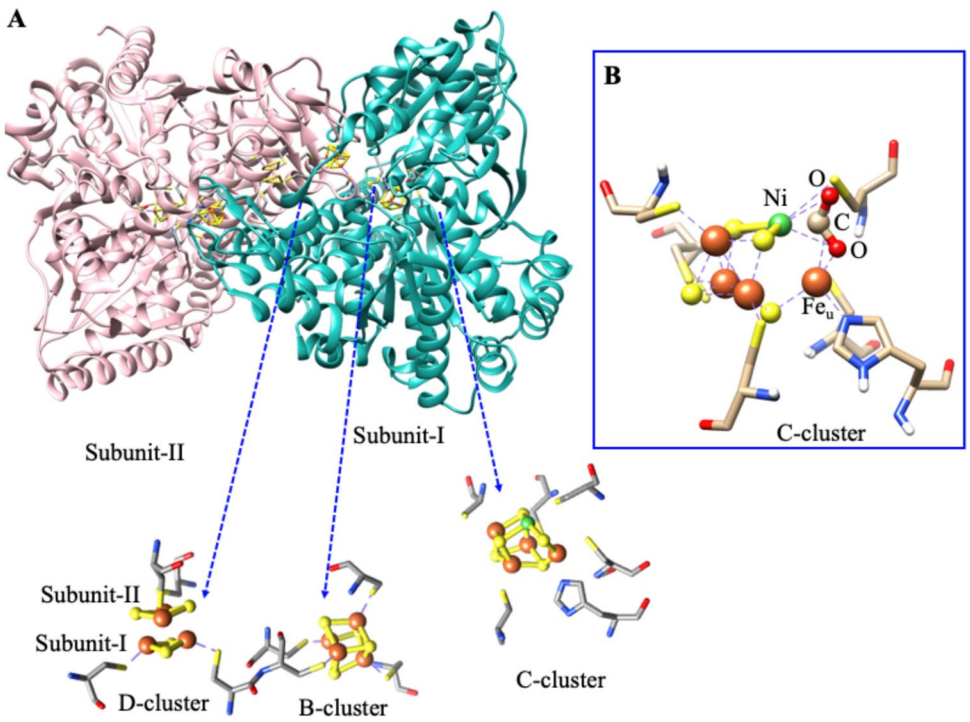

Fig. 8 **A** The Crystal structure of the [NiFe]-CODH homodimer (PDB:1SU6) from *C. hydrogenoformans and t*he metal-sulfur clusters are highlighted. **B** Crystal structure of the C-cluster of CO_2 bound [NiFe]-CODH (PDB: 4UDX) from *C. hydrogenoformans*. Fe (red ball); Ni (green ball), and S (yellow ball)

coupling between the Ni center and the FeS cluster in the redox regulation of CO_2 binding and release [6, 102, 116].

Magnetic interactions and enzymatic function in Ni, Mo, Cu-containing complex enzymes

Magnetic interactions in metal enzymes are direct manifestations of unpaired electron spins residing in transition metal centers or iron-sulfur clusters. These interactions are tightly correlated with redox chemistry, substrate binding, catalytic turnover, and electron transfer (ET) dynamics, all of which are fundamental to enzymatic activity. EPR and related spectroscopic tools proved as essential for studying these interactions and to characterize electron transfer processes in catalytically active redox states and electron transfer sites.

[NiFe]-hydrogenases

The [NiFe] are bimetallic active sites are coupled with iron-sulfur (Fe/S) clusters that serve as electron relays [41]. In catalytically relevant states (e.g., Ni-C, Ni-L), magnetic interactions between unpaired d-electrons and surrounding nuclei (such as protons or Fe/S centers) can be observed by EPR and ENDOR [50–60]. The magnetic coupling between the metal center and nearby [4Fe4S] clusters controls electron flux to and from the active site, directly modulating H_2 production or oxidation [50–60]. Subtle changes in hyperfine couplings reflect protonation events, which are part of the proton-coupled electron transfer (PCET) mechanism central to catalysis [46, 62]. Indeed, the Fe in the [NiFe] active site is primarily redox inactive, but shows hyperfine couplings influenced by the nature of its ligands, like CO and CN^-. Ligand substitution impacts on the Fe-centre, affecting magnetic coupling to the Ni center [46, 47]. In addition, EPR values of variable redox states of the Ni–C (H-bound) and Ni–L (light-induced) reveal significant changes in Ni-hyperfine coupling due to alterations in spin density and ligand binding [31–33, 54]. These couplings may provide critical insights into the electronic and geometric environment of the active site, which can lead to the design of synthetic catalysts that efficiently activate hydrogen.

Mo containing enzymes (xanthine oxidase family)

These enzymes contain mononuclear Mo centers coordinated by sulfur ligands and dithiolene cofactors (like MPT) [64]. During catalysis, Mo cycles between Mo(VI), Mo(V), and Mo(IV) oxidation states. The Mo(V) intermediate is EPR-active and often stabilized by spin coupling with surrounding centers (e.g., FeS clusters or Cu centers in certain oxidases). Magnetic interactions in Mo(V) states reveal the electronic structure and geometry of the active site, giving insights into substrate binding orientation and electron delocalization [67, 68, 72]. In enzymes like aldehyde oxidase or xanthine oxidase, the strength of magnetic interactions often correlates with the efficiency of oxidative transformations. Indeed, several inhibitors of the XO.

family, such as arsenite, formaldehyde, glycerol and ethylene glycol interact with the Mo-site to yield Mo(V)-inhibitor complex, which changes in the electronic structure of the Mo(V) site, favoring a larger magnetic coupling with the proximal FeS center compared to dithionite-reduced *Dg*AOR [76, 117]. These inhibited enzyme states are vital for understanding changes in the integrity of the electron transfer chain upon inhibition and providing insights that can guide the rational design of drugs.

Carbon monoxide dehydrogenase (CODH)

Generally, CODHs are two classes: [MoCu]-CODHs and [NiFe]-CODHs. [MoCu]-CODH belongs to the xanthine oxidase family, containing an unprecedented heterobimetallic cluster, [Mo–S–Cu] cluster. In catalytic cycle, Mo(V) is generated and shows a rhombic EPR signal with strong hyperfine coupling to Cu-nuclei [101] and even Cu substituted Ag-Mo-CODH shows Mo(V) EPR signal with strong hyperfine coupling to Ag-nuclei, suggesting that CO binds Cu-site, triggering electron density to Mo-site for activation of CO across the Mo–S–Cu motif [101]. Moreover, the Ag-substituted CODH exhibits a slow enzymatic activity, indicating that substitution of the native metal by other non-native metals alters the electron flow in the catalytic pathway, providing valuable insights to design artificial catalysts that can modulate the activity.

The other class of CODH is [NiFe]-CODH C-cluster containing [Ni4Fe5S] and CO_2-bound C-cluster, [Ni4Fe4S(CO_2)], which represents a catalytic intermediate [6, 102]. The CO_2 binding C-cluster significantly changes g-values, suggesting that substrate binding modulates the magnetic interactions between Ni and Fe centers and therefore, the CO_2-bound C-cluster state leads to the cleavage of the C–O bond in CO_2, yielding Ni–CO and Fe_u–OH species [116, 118]. This CO_2-bound intermediate provides a blueprint for designing catalysts that can efficiently activate CO and CO_2.

EPR spectroscopy reveals redox transitions involving Ni(II)/Ni(I), coupled with Fe-S oxidation changes. The magnetic interaction between Ni and Fe/S centers enables rapid electron redistribution, essential for breaking the strong C≡O bond in CO. In CODH/ACS (acetyl-CoA synthase complex), inter-cluster magnetic coupling (between the C-cluster and the A-cluster) aligns with conformational changes that facilitate substrate channelling and catalysis [112, 119].

Final remarks

Although out of the scope of this review, MoFe Nitrogenases [1, 120] and Copper Enzymes (LPMO (lytic polysaccharide monooxygenases), Azurin, Cytochrome c Oxidase) [10, 121] are also case studies of this type of interactions. The MoFe protein contains the FeMo-cofactor ([FeMoSC]) at the active site. It is electronically complex and paramagnetic in several redox states (e.g., E_0, E_4). Magnetic interactions are crucial in stabilizing and identifying intermediates during the 8-electron reduction of N_2 to NH_3 [122].

The E4 "Janus intermediate", containing two bridging hydrides, shows a unique EPR signature reflecting spin delocalization across multiple metal centers. Spin-coupled Fe/S clusters (P-cluster, Fe protein) deliver electrons sequentially—these steps are regulated by precise magnetic interactions that affect timing and directionality of ET. The EPR, ENDOR, and Mössbauer studies of nitrogenase show how the magnetic structure controls substrate binding, activation, and releasing [1, 120, 123–129].

Mononuclear Cu(II) centers, such as LPMO, Azurin, and Cytochrome c Oxidase are often EPR-active, and magnetic anisotropy (g-tensor) gives detailed information about geometry and ligand field. In LPMOs Cu(II)/Cu(I) cycling, driven by reductants and oxygen, is tightly linked to magnetic properties observed in EPR. Magnetic coupling between Cu and adjacent redox cofactors (like tyrosyl radicals or Fe centers in multi-domain oxidases) can modulate the redox potential and catalytic cycle [10, 121, 130–132].

Conclusions

Magnetic interactions between Fe/S clusters and other metal centers, such as nickel and molybdenum, play a pivotal role in defining the catalytic efficiency, redox properties, and structural stability of key metalloenzymes. The intricate electronic coupling and spin exchange mechanisms modulate enzymatic function.

In all these enzymes, magnetic interactions are not peripheral—they reflect and influence the core chemical transformations taking place. These interactions: (i) serve as spectroscopic fingerprints for redox intermediates, (ii) indicate electron transfer pathways and their directionality, and (iii) provide mechanistic insight into substrate binding, bond cleavage, and product release, influencing the thermodynamic and kinetic parameters of catalysis.

Understanding these magnetic features is an interesting and stimulating theoretical problem, but also directly informs enzyme engineering, biocatalyst design, and the development of biomimetic catalysts for energy conversion and environmental remediation.

Advances in spectroscopic techniques, including electron paramagnetic resonance and Mössbauer spectroscopy, along with computational modelling, have significantly deepened our understanding of these interactions at the molecular level.

By elucidating the fundamental principles governing these magnetic interactions, insights may contribute not only to the field of bioinorganic chemistry but also to the rational design of biomimetic catalysts with potential applications in renewable energy, biotechnology, and industrial catalysis. Future research integrating experimental and theoretical approaches will further refine our comprehension of metalloenzyme function, paving the way for innovative strategies in enzyme engineering and sustainable catalysis.

Acknowledgements BKM thanks to DST−SERB for the CRG grant (file no CRG/2022/005673) and the Cluster University of Jammu for providing infrastructure facilities. This work was also supported by the PTDC/BTA-BTA/0935/2020 project and also by the Associate Laboratory for Green Chemistry—LAQV (UIDB/50006/2020 and UIDP/50006/2020), which are financed by national funds from Fundacão para a Ciência e a Tecnologia, MCTES (FCT/MCTES).

Author Contributions All authors discussed and contributed to the final manuscript. JJGM: initial outline, writing, and editing the manuscript. BKM: writing and editing the manuscript. IM: writing and editing the manuscript.

Funding Open access funding provided by FCT|FCCN (b-on). Funding from DST–SERB, India for the CRG grant (CRG/2022/005673), and Fundacão para a Ciência e a Tecnologia, MCTES (FCT/MCTES), Portugal, (PTDC/BTA-BTA/0935/2020 and LAQV (UIDB/50006/2020 and UIDP/50006/2020).

Data availability No datasets were generated or analysed during the current study.

Declarations

Conflict of interest The authors declare no competing interests.

Ethical approval and consent to participate Not applicable.

Consent for publication Not applicable.

References

1. Einsle O, Rees DC (2020) Structural enzymology of nitrogenase enzymes. Chem Rev 120:4969–5004
2. Schmidt FV, Schulz L, Zarzycki J, Prinz S, Oehlmann NN, Erb TJ, Rebelein JG (2024) Structural insights into the iron nitrogenase complex. Nat Struct Mol Biol 31:150–158
3. Maiti BK (2022) Cross-talk between (hydrogen) sulfite and metalloproteins: impact on human health. Chem Eur J 28:e202104342
4. Maiti BK, Maia LB, Moura JJG (2022) Sulfide and transition metals—a partnership for life. J Inorg Biochem 227:111687
5. Maiti BK, Moura I, Moura JJG (2024) Molybdenum-copper antagonism in metalloenzymes and anti-copper therapy. ChemBioChem 25:e202300679
6. Stripp ST, Duffus BR, Fourmond V, Léger FC, Leimkühler S, Hirota S, Hu Y, Jasniewski A, Ogata H, Ribbe MW (2022) Second and outer coordination sphere effects in nitrogenase, hydrogenase, formate dehydrogenase, and CO dehydrogenase. Chem Rev 122:11900–11973
7. Lubitz W, Ogata H, Rudiger O, Reijerse E (2014) Hydrogenases. Chem Rev 114:4081–4148
8. Hille R, Hall J, Basu P (2014) The mononuclear molybdenum enzymes. Chem Rev 114:3963–4038
9. Maia LB, Moura I, Moura JJG (2017) Chap 1 molybdenum and tungsten-containing enzymes—an overview. In: Hille R, Schulzke C, Kirk ML (eds) Molybdenum and Tungsten Enzymes: Biochemistry RSC Metallobiology Series No. 5. The Royal Society of Chemistry, Cambridge, pp 1–80
10. Can M, Armstrong FA, Ragsdale SW (2014) Structure, function, and mechanism of the nickel metalloenzymes, CO dehydrogenase, and acetyl-COA synthase. Chem Rev 114:4149–4174
11. Lewis LC, Sanabria-Gracia JA, Lee Y, Jenkins AJ, Shafaat HS (2024) Electronic isomerism in a heterometallic nickel–iron–sulfur cluster models substrate binding and cyanide inhibition of carbon monoxide dehydrogenase. Chem Sci 15:5916–5928
12. Zhang B, Hemann CF, Hille R (2010) Kinetic and spectroscopic studies of the molybdenum-copper CO dehydrogenase from *Oligotropha carboxidovorans*. J Biol Chem 285:12571–12578
13. Moura JJG, et al. (1988) in Bioinorganic Chemistry of Nickel, ed. Lancaster Jr. JR, VCH Publishers, Deerfield Beach (in press)
14. Stappen CV, Decamps L, Cutsail GE III, Bjornsson R, Henthorn JT, Birrell JA, DeBeer S (2020) The spectroscopy of nitrogenases. Chem Rev 120:5005–5081
15. Holm RH, Lo W (2016) Structural conversions of synthetic and protein-bound iron-sulfur clusters. Chem Rev 116:13685–13713
16. Lubitz W, Reijerse E, Mv G (2007) [NiFe] and [FeFe] hydrogenases studied by advanced magnetic resonance techniques. Chem Rev 107:4331–4365
17. Goámez MC, Neuman NI, Dalosto SD, González PJ, Moura JJG, Rizzi AC, Brondino CD (2015) Isotropic exchange interaction between Mo and the proximal FeS center in the xanthine oxidase family member aldehyde oxidoreductase from *Desulfovibrio gigas* on native and polyalcohol inhibited samples: an EPR and QM/MM study. J Biol Inorg Chem 20:233–242
18. Peters JW, Lanzilotta WN, Lemon BJ, Seefeldt LC (1998) X-ray crystal structure of the Fe-only hydrogenase (CpI) from *Clostridium pasteurianum* to 1.8 angstrom resolution. Science 282:1853–1858
19. Esselborn J, Muraki N, Klein K, Engelbrecht V, Metzler-Nolte N, Apfel U-P, Hofmann E, Kurisu G, Happe T (2016) A structural view of synthetic cofactor integration into [FeFe]-hydrogenases. Chem Sci 7:959–968
20. Ogata H, Nishikawa K, Lubitz W (2015) Hydrogens detected by subatomic resolution protein crystallography in a [NiFe] hydrogenase. Nature 520:571–574
21. Volbeda A, Martin L, Cavazza C, Matho M, Faber BW, Roseboom W, Albracht SP, Garcin E, Rousset M, Fontecilla-Camps JC (2005) Structural differences between the ready and unready oxidized states of [NiFe] hydrogenases. J Biol Inorg Chem 10:239–249
22. Marques MC, Tapia C, Gutiérrez-Sanz O, Ramos AR, Keller KL, Wall JD, Lacey ALD, Matias PM, Pereira IC (2017) The direct role of selenocysteine in [NiFeSe] hydrogenase maturation and catalysis. Nat Chem Biol 13:544–550
23. Garcin E, Vernede X, Hatchikian EC, Volbeda A, Frey M, Fontecilla-Camps JC (1999) The crystal structure of a reduced [NiFeSe] hydrogenase provides an image of the activated catalytic center. Structure 7:557–566
24. Huang G, Wagner T, Wodrich MD, Ataka K, Bill E, Ermler U, Hu X, Shima S (2019) The atomic-resolution crystal structure of activated [Fe]-hydrogenase. Nat Catal 2:537–543
25. Volbeda A, Charon M-H, Piras C, Hatchikian EC, Frey M, Fontecilla-Camps JC (1995) Crystal structure of the nickel–iron hydrogenase from Desulfovibrio gigas. Nature 373:580
26. Frielingsdorf S, Fritsch J, Schmidt A, Hammer M, Löwenstein J, Siebert E, Pelmenschikov V, Jaenicke T, Kalms J, Rippers Y, Lendzian F, Zebger I, Teutloff C, Kaupp M, Bittl R, Hildebrandt P, Friedrich B, Lenz O, Scheerer P (2014) Reversible [4Fe-3S] cluster morphing in an O2-tolerant [NiFe] hydrogenase. Nat Chem Biol 10:378–385
27. Teixeira M, Moura I, Xavier AV, Moura JJG, LeGall J, DerVartanian DV, Peck HD Jr, Huyn BH (1989) Redox intermediates of *Desulfovibrio gigus* [NiFe] hydrogenase generated under hydrogen. J Biol Chem 264:16435–16450
28. Fauque G, Peck HD Jr, Moura JJG, Huynh BH, Berlier Y, DerVartanian DV, Teixeria M, Przybyla AE, Lespinat PA, Moura I, LeGall J (1988) The three classes of hydrogenases from sulfate-reducing bacteria of the genus Desulfovibrio. FEMS Microbiol Rev 54:299–344
29. Moura JJG, Moura I, Huynh BH, Kriiger HJ, Teixeria M, DuVarney RC, DerVartanian DV, Xavier AV, Peck HD Jr, LeGall J (1982) Unambiguous identification of the nickel EPR signal in 61Ni-enriched *Desulfovibrio gigas* hydrogenase. Biochem Biophys Res Commun 108:1388–1393
30. Teixeria M, Moura I, Xavier AV, DerVartanian DV, LeGall J, Peck HD Jr, Huynh BH, Moura JJG (1983) Desulfouibn'o gigas hydrogenase : redox properties of the nickel and iron–sulfur centers. Eur J Biochem 130:481–484
31. Moura JJG, Teixeira M, Moura I, Xavier AV, LeGall J (1984) Nickel—a redox catalytic site in hydrogenase. J Mol Catal 23:303–314
32. Teixeira M, Moura I, Xavier AV, Huynh BH, DerVartanian DV, Peck HD Jr, Le Gall J, Moura JG (1985) Electron paramagnetic resonance studies on the mechanism of activation and the catalytic cycle of the nickel-containing hydrogenase from *Desulfovibrio gigas*. J Biol Chem 260:8942–8950
33. Huynh BH, Patil DS, Moura I, Teixeira M, Moura JJG, DerVartanien DV, Czechowski MH, Prickril BC, Peck HD Jr, LeGall J (1986) On the active sites of the [NiFe] hydrogenase from *Desulfovibrio gigas*. Mössbauer and redox-titration studies. J Biol Chem 262:795–800
34. Cammack R, Patil DS, Aguirre R, Hatchikian EC (1982) Redox properties of the ESR-detectable nickel in hydrogenase from *Desulfovibrio gigas*. FEBS Lett 142:289–292
35. Fernandez VM, Hatchikian EC, Patil DS, Cammack R (1986) ESR-detectable nickel and iron–sulphur centres in relation to the reversible activation of Desulfovibrio gigas hydrogenase. Biochim Biophys Acta 883:145–154

36. Cammack R, Patil DS, Hatchikian EC, Fernandez VM (1987) Nickel and iron-sulphur centers in *Desulfovibrio gigas* hydrogenase: ESR spectra, redox properties and interactions. Biochim Biophys Acta 912:98–109
37. Roncaroli F, Bill E, Friedrich B, Lenz O, Lubitz W, Pandelia M-E (2015) Cofactor composition and function of a H2-sensing regulatory hydrogenase as revealed by Mössbauer and EPR spectroscopy. Chem Sci 6:4495–4507
38. Lacey ALD, Fernández VM, Rousset M, Cammack R (2007) Activation and inactivation of hydrogenase function and the catalytic cycle: spectroelectrochemical studies. Chem Rev 107:4304–4330
39. Mv G, Stein M, Brecht M, Schröder O, Lendzian F, Bittl R, Ogata H, Higuchi Y, Lubitz W (2006) A single-crystal ENDOR and density functional theory study of the oxidized states of the [NiFe] hydrogenase from *Desulfovibrio vulgaris* Miyazaki F. J Biol Inorg Chem 11:41–51
40. Maia LB, Maiti BK, Moura I, Moura JJG (2024) Selenium—more than just a fortuitous sulfur substitute in redox biology. Molecules 29:120
41. Ogata H, Hirota S, Nakahara A, Komori H, Shibata HN, Kato T, Kano K, Higuchi Y (2005) Activation process of [NiFe] hydrogenase elucidated by high-resolution X-ray analyses: conversion of the ready to the unready state. Structure 13:1635–1642
42. Ogata H, Lubitz W, Higuchi Y (2009) [NiFe] hydrogenases: structural and spectroscopic studies of the reaction mechanism. Dalton Trans 37:7577–7587
43. Yagi T, Higuchi Y (2013) Studies on hydrogenase. Proc Jpn Acad Ser B 89:16–33
44. de Lacey AL, Hatchikian EC, Volbeda A, Frey M, Fontecilla-Camps JC, Fernandez VM (1997) Infrared-spectroelectrochemical characterization of the [NiFe] hydrogenase of *Desulfovibrio gigas*. J Am Chem Soc 119:7181–7189
45. Pardo A, De Lacey AL, Fernandez VM, Fan H-J, Fan Y, Hall MB (2006) Density functional study of the catalytic cycle of nickel–iron [NiFe] hydrogenases and the involvement of high-spin nickel(II). J Biol Inorg Chem 11:286–306
46. Ash PA, Hidalgo R, Vincent KA (2017) Proton transfer in the catalytic cycle of [NiFe] hydrogenases: insight from vibrational spectroscopy. ACS Catal 7:2471–2485
47. Stripp ST (2021) In situ infrared spectroscopy for the analysis of gas-processing metalloenzymes. ACS Catal 11:7845–7862
48. Albracht SPJ, Kalkman ML, Slater EC (1983) Magnetic interaction of nickel(III) and the iron-sulphur cluster in hydrogenase from *Chromatium vinosum*. Biochim Biophys Acta 724:309–316
49. LeGall J, Ljungdahl PO, Moura I, Peck HD Jr, Xavier AV, Moura JJG, Teixera M, Huynh BH, DerVartanian DV (1982) The presence of redox-sensitive nickel in the periplasmic hydrogenase from *Desulfovibrio gigas*. Biochem Biophys Res Commun 106:610–616
50. Barilone JL, Ogata H, Lubitz W, van Gastel M (2015) Structural differences between the active sites of the Ni-A and Ni-B states of the [NiFe] hydrogenase: an approach by quantum chemistry and single crystal ENDOR spectroscopy. Phys Chem Chem Phys 17:16204–16212
51. Moura JJG, Teiera M, Moura I (1989) Theroleofnickelandiron-sulfur centersinthe bioproduction of hydrogen. Pure & Appl Chem 61:915–921
52. Moura JJG, LeGall J, Xavier AV (1984) Interconversion from 3Fe into 4Fe clusters in the presence of *Desulfovibrio gigas* cell extracts. Eur J Biochem 141:319–322
53. Papaefthymiou V, Girerd JJ, Moura I, Moura JJG, Muenck E (1987) Moessbauer study of *D. gigas* ferredoxin II and spin-coupling model for Fe3S4 cluster with valence delocalization. J Am Chem Soc 109:4703–4710
54. Schneider K, Schlegel HG, Jochim K (1984) Effect of nickel on activity and subunit composition of purified hydrogenase from *Nocardia opaca*. Eur Biochem 138:533–541
55. Wang H, Yoda Y, Ogata H, Tanaka Y, Lubitz W (2015) A strenuous experimental journey searching for spectroscopic evidence of a bridging nickel–iron-hydride in [NiFe] hydrogenase. J Synchrotron Radiat 22:1334–1344
56. Karafoulidi-Retsou C, Lorent C, Katz S, Rippers Y, Matsuura H, Higuchi Y, Zebger I, Horch M (2014) Light-induced electron transfer in a [NiFe] hydrogenase opens a photochemical shortcut for catalytic dihydrogen cleavage. Angew Chem Int 63:e202409065
57. Chambers GM, Huynh MT, Li Y, Hammes-Schiffer S, Rauchfuss TB, Reijerse E, Lubitz W (2016) Models of the Ni-L and Ni-SIa states of the [NiFe]-hydrogenase active site. Inorg Chem 55:419–431
58. Brecht M, Mv G, Buhrke T, Friedrich B, Lubitz W (2003) Direct detection of a hydrogen ligand in the [NiFe] center of the regulatory H2-sensing hydrogenase from *Ralstonia eutropha* in its reduced state by HYSCORE and ENDOR spectroscopy. J Am Chem Soc 125:13075–13083
59. Foerster S, van Gastel M, Brecht M, Lubitz W (2005) An orientation-selected ENDOR and HYSCORE study of the Ni-C active state of *Desulfovibrio vulgaris* Miyazaki F hydrogenase. J Biol Inorg Chem 10:51–62
60. Carepo M, Tierney DL, Brondino CD, Yang TC, Pamplona A, Telser J, Moura I, Moura JJG, Hoffman BM (2002) 17O ENDOR detection of a solvent-derived Ni−(OHx)−Fe bridge that is lost upon activation of the hydrogenase from *Desulfovibrio gigas*. J Am Chem Soc 124:281–286
61. Cammack R, Fernandez VM, Schneider K (1986) Activation and active sites of nickel-containing hydrogenases. Biochimie 68:85–91
62. Lespinat PA, Berlier Y, Fauque G, Czechowski M, Dimon B, Le Gall J (1986) The pH dependence of proton-deuterium exchange, hydrogen production and uptake catalyzed by hydrogenases from sulfate-reducing bacteria. Biochimie 68:55–61
63. Guigliarelli B, More C, Fournel A, Asso M, Hatchikian EC, Williams R, Cammack R, Bertrand P (1995) Structural organization of the Ni and (4Fe–4S) centers in the active form of *Desulfovibrio gigas* hydrogenase. Analysis of the magnetic interactions by electron paramagnetic resonance spectroscopy. Biochemistry 34:4781–4790
64. Moura JJG (2023) The history of *Desulfovibrio gigas* aldehyde oxidoreductase—a personal view. Molecules 28:4229
65. Enroth C, Eger BT, Okamoto K, Nishino T, Nishino T, Pai EF (2000) Crystal structures of bovine milk xanthine dehydrogenase and xanthine oxidase: structure-based mechanism of conversion. Proc Natl Acad Sci USA 97:10723–10728
66. Brondino CD, Romão MJ, Moura I, Moura JJG (2006) Molybdenum and tungsten enzymes: the xanthine oxidase family. Curr Opin Chem Biol 10:109–114
67. Thapper A, Rivas MG, Brondino CD, Ollivier B, Fauque G, Moura I, Moura JJG (2006) Biochemical and spectroscopic characterization of an aldehyde oxidoreductase isolated from *Desulfovibrio aminophilus*. J Inorg Biochem 100:44–50
68. Andrade SL, Brondino CD, Feio MJ, Moura I, Moura JJG (2000) Aldehyde oxidoreductase activity in *Desulfovibrio alaskensis* NCIMB 13491 EPR assignment of the proximal [2Fe-2S] cluster to the Mo site. Eur J Biochem 267:2054–2061
69. Romão MJ, Archer M, Moura I, Moura JJG, LeGall J, Engh R, Schneider M, Hof P, Huber R (1995) Crystal structure of the xanthine oxidase-related aldehyde oxido-reductase from *D. gigas*. Science 270:1170–1176
70. Rebelo J, Dias J, Huber R, Moura JJG, Romão MJ (2001) Structure refinement of the aldehyde oxidoreductase from

Desulfovibrio gigas (MOP) at 1.28 Å. J Biol Inorg Chem 6:791–800
71. Barber MJ, Salerno JC, Siegel LM (1982) Magnetic interactions in milk xanthine oxidase. Biochemistry 21:1648–1656
72. Lowe DJ, Bray R (1978) Magnetic coupling of the molybdenum and iron–sulphur centres in xanthine oxidase and xanthine dehydrogenases. Biochem J 169:471–479
73. Turner N, Barata B, Bray RC, Deistung J, LeGall J (1987) The molybdenum iron–sulphur protein from *Desulfovibrio gigas* as a form of aldehyde oxidase. Biochem J 243:755–761
74. Duarte RO, Archer M, Dias JM, Bursakov S, Huber R, Moura I, Romão MJ, Moura JJG (2000) Biochemical-spectroscopy characterization and preliminary X-ray analysis of a new aldehyde oxidoreductase isolated from *Desulfovibrio desulfuricans* ATTC 27774. Biochem Biophys Res Commun 24:745–749
75. González PJ, Barrera GI, Rizzi AC, Moura JJG, Passeggi MCG, Brondino CD (2009) EPR studies of the Mo-enzyme aldehyde oxidoreductase from *Desulfovibrio gigas*: an application of the Bloch–Wangsness–Redfield theory to a system containing weakly-coupled paramagnetic redox centers with different relaxation rate. J Inorg Biochem 103:1342–1346
76. Santos-Silva T, Ferroni F, Thapper A, Marangon J, González PJ, Rizzi AC, Moura I, Moura JJG, Romão MJ, Brondino CD (2009) Kinetic, structural, and EPR studies reveal that aldehyde oxidoreductase from *Desulfovibrio gigas* does not need a sulfido ligand for catalysis and give evidence for a direct Mo−C interaction in a biological system. J Am Chem Soc 131:7990–7998
77. Hille R (2010) EPR studies of xanthine oxidoreductase and other molybdenum-containing hydroxylases. In: Hanson G, Berliner L (eds) Metals in Biology. Biological Magnetic Resonance, vol 29. Springer, New York
78. Brondino CD, Rivas MG, Romão MJ, Moura JJG, Moura I (2006) Structural and electron paramagnetic resonance (EPR) studies of mononuclear molybdenum enzymes from sulfate-reducing bacteria. Acc Chem Res 39:788–796
79. Bray RC, Turner NA, Le Gall J, Barata BAS, Moura JJG (1991) Information from EPR spectroscopy on the iron-sulphur centres of the iron-molybdenum protein (aldehyde oxidoreductase) of *Desulfovibrio gigas*. Biochem J 280:817–820
80. Moura JJG, Xavier AV, Cammack R, Hall DO, Bruschi M, Le Gall J (1978) Oxidation-reduction studies of the Mo-(2Fe-2S) protein from *Desulfovibrio gigas*. Biochem J 173:419–425
81. Barata BAS, Liang J, Moura I, LeGall J, Moura JJG, Huynh HB (1992) Mössbauer study of the native, reduced and substrate-reacted *Desulfovibrio gigas* aldehyde oxido-reductase. Eur J Biochem 204:773–778
82. Caldeira J, Belle V, Asso M, Guigliarelli B, Moura I, Moura JJG, Bertrand P (2000) Analysis of the electron paramagnetic resonance properties of the [2Fe-2S]1+ centers in molybdenum enzymes of the xanthine oxidase family: assignment of signals I and II. Biochemistry 39:2700–2707
83. More C, Asso M, Roger G, Guigliarelli B, Caldeira J, Moura JJG, Bertrand P (2005) Study of the spin-spin interactions between the metal centers of *Desulfovibrio gigas* aldehyde oxidoreductase: Identification of the reducible sites of the [2Fe–2S]1+,2+ cluster. Biochemistry 44:11628–11635
84. Maia LB, Moura I, Moura JJG (2017) EPR spectroscopy on mononuclear molybdenum-containing enzymes. In: Hanson G, Berliner L (eds) Future Directions in Metalloprotein and Metalloenzyme Research. Biological Magnetic Resonance, vol 33. Springer, Cham
85. Jeoung J-H, Dobbek H (2007) Carbon dioxide activation at the Ni,Fe-cluster of anaerobic carbon monoxide dehydrogenase. Science 318:1461–1464
86. Dobbek H, Gremer L, Kiefersauer R, Huber R, Meyer O (2002) Catalysis at a dinuclear [CuSMo(O)OH] cluster in a CO dehydrogenase resolved at 1.1-Å resolution. Proc Natl Acad Sci USA 99:15971–15976
87. Hille R, Dingwall S, Wilcoxen J (2015) The aerobic CO dehydrogenase from *Oligotropha carboxidovorans*. J Biol Inorg Chem 20:243–251
88. Xavier JC, Preiner M, Martin WF (2018) Something special about CO-dependent CO2 fixation. FEBS J 285:4181–4195
89. Ensign SA (1995) Reactivity of carbon monoxide dehydrogenase from *Rhodospirillum rubrum* with carbon dioxide, carbonyl sulfide, and carbon disulphide. Biochemistry 34:5372–5381
90. Svetlitchnyi V, Peschel C, Acker G, Meyer O (2001) Two membrane-associated NiFeS-carbon monoxide dehydrogenases from the anaerobic carbon-monoxide-utilizing eubacterium *Carboxydothermus hydrogenoformans*. J Bacteriol 183:5134–5144
91. Gnida M, Ferner R, Gremer L, Meyer O, Meyer-Klaucke W (2003) A novel binuclear [CuSMo] cluster at the active site of carbon monoxide dehydrogenase: characterization by X-ray absorption spectroscopy. Biochemistry 42:222–230
92. Dobbek H, Gremer L, Meyer O, Huber R (1999) Crystal structure and mechanism of CO dehydrogenase, a molybdo iron–sulfur flavoprotein containing S-selanylcysteine. Proc Natl Acad Sci USA 96:8884–8889
93. Gourlay C, Nielsen DJ, White JM, Knottenbelt SZ, Kirk ML, Young CG (2006) Paramagnetic active site models for the molybdenum-copper carbon monoxide dehydrogenase. J Am Chem Soc 128:2164–2165
94. Shanmugam M, Wilcoxen J, Habel-Rodriguez D, Cutsail GE III, Kirk ML, Hoffman BM, Hille R (2013) 13C and 63,65Cu ENDOR studies of CO dehydrogenase from *Oligotropha carboxidovorans*. experimental evidence in support of a copper-carbonyl intermediate. J Am Chem Soc 135:17775–17782
95. Steina BW, Kirk ML (2014) Orbital contributions to CO oxidation in Mo–Cu carbon monoxide dehydrogenase. Chem Commun 50:1104–1106
96. Xua K, Hirao H (2018) Revisiting the catalytic mechanism of Mo–Cu carbon monoxide dehydrogenase using QM/MM and DFT calculations. Phys Chem Chem Phys 20:18938–18948
97. Rovaletti A, Bruschi M, Moro G, Cosentino U, Ryde U, Greco CA (2019) Thiocarbonate sink on the enzymatic energy landscape of aerobic CO oxidation? Answers from DFT and QM/MM models of Mo–Cu CO-dehydrogenases. J Catal 372:201–205
98. Meyer O, Frunzke K, Gadkari D, Jacobitz S, Hugendieck I, Kraut M (1990) Utilization of carbon monoxide by aerobes: recent advances. FEMS Microbiol Rev 87:253–260
99. Pelzmann A, Ferner M, Gnida M, Meyer-Klaucke W, Maisel T, Meyer O (2009) The CoxD protein of *Oligotropha carboxidovorans* is a predicted AAA+ ATPase chaperone involved in the biogenesis of the CO dehydrogenase [CuSMoO2] cluster. J Biol Chem 284:9578–9586
100. Resch M, Dobbek H, Meyer O (2005) Structural and functional reconstruction in situ of the [CuSMoO2] active site of carbon monoxide dehydrogenase from the carbon monoxide oxidizing eubacterium *Oligotropha carboxidovorans*. J Biol Inorg Chem 10:518–528
101. Wilcoxen J, Snider S, Russ Hille R (2011) Substitution of silver for copper in the binuclear Mo/Cu center of carbon monoxide dehydrogenase from *Oligotropha carboxidovorans*. J Am Chem Soc 133:12934–12936
102. Basak Y, Jeoung J-H, Domnik L, Ruickoldt J, Dobbek H (2022) Substrate activation at the Ni,Fe cluster of CO dehydrogenases: the influence of the protein matrix. ACS Catal 12:12711–12719
103. Dobbek H, Svetlitchnyi V, Gremer L, Huber R, Meyer O (2001) Crystal structure of a carbon monoxide dehydrogenase reveals a [Ni-4Fe-5S] cluster. Science 293:1281–1285

104. Dobbek H, Svetlitchnyi V, Liss J, Meyer O (2004) Carbon monoxide dehydrogenase from *Carboxydothermus hydrogenoformans*: CO reduced state. J Am Chem Soc 126:5382–5387
105. Drennan CL, Heo J, Sintchak MD, Schreiter E, Ludden PW (2001) Life on carbon monoxide: X-ray structure of *Rhodospirillum rubrum* Ni–Fe–S carbon monoxide dehydrogenase. Proc Natl Acad Sci USA 98:11973–11978
106. Doukov TI, Iverson TM, Seravalli J, Ragsdale SW, Drennan CL (2002) A Ni–Fe–Cu center in a bifunctional carbon monoxide dehydrogenase/acetyl-CoA synthase. Science 298:567–572
107. Darnault C, Volbeda A, Kim EJ, Legrand P, Vernede X, Lindahl PA, Fontecilla-Camps JC (2003) Ni–Zn–[Fe4–S4] and Ni–Ni–[Fe4–S4] clusters in closed and open α subunits of acetyl-CoA synthase/carbon monoxide dehydrogenase. Nat Struct Biol 10:271–279
108. Hu Z, Spangler NJ, Anderson ME, Xia J, Ludden PW, Lindahl PA, Munck E (1996) Nature of the C-cluster in Ni-containing carbon monoxide dehydrogenases. J Am Chem Soc 118:830–845
109. Carlson ED, Papoutsakis ET (2017) Heterologous expression of the *Clostridium carboxidivorans* CO dehydrogenase alone or together with the acetyl coenzyme A synthase enables both reduction of CO2 and oxidation of CO by *Clostridium acetobutylicum*. Appl Environ Microbiol 83:e00829
110. Fesseler J, Jeoung J-H, Dobbek H (2015) How the [NiFe4S4] cluster of CO dehydrogenase activates CO2 and NCO(–). Angew Chem Int Ed Engl 54:8560–8564
111. Wittenborn EC, Merrouch M, Ueda C et al (2018) Redox-dependent rearrangements of the nifes cluster of carbon monoxide dehydrogenase. Elife 7:e39451
112. Heo J, Staples CR, Telser J, Ludden PW (1999) Rhodospirillum rubrum CO-dehydrogenase. Part 2. Spectroscopic investigation and assignment of spin−spin coupling signals. J Am Chem Soc 121:11045–11057
113. Amara P, Mouesca J-M, Volbeda A, Fontecilla-Camps JC (2011) Carbon monoxide dehydrogenase reaction mechanism: a likely case of abnormal CO2 insertion to a Ni–H– bond. Inorg Chem 50:1868–1878
114. Ralston CY, Wang H, Ragsdale SW, Kumar M, Spangler NJ, Ludden PW, Gu W, Jones RM, Patil DS, Cramer SP (2000) Characterization of heterogeneous nickel sites in CO dehydrogenases from *Clostridium thermoaceticum* and *Rhodospirillum rubrum* by Nickel L-edge X-ray spectroscopy. J Am Chem Soc 122:10553–10560
115. Gu W, Seravalli J, Ragsdale SW, Cramer SP (2004) CO-induced structural rearrangement of the C cluster in *Carboxydothermus hydrogenoformans* CO dehydrogenase-evidence from Ni K-edge X-ray absorption spectroscopy. Biochemistry 43:9029–9035
116. Breglia R, Arrigoni F, Sensi M, Greco C, Fantucci P, Gioia LD, Bruschi M (2021) Inorg Chem 60:387–402
117. Shanmugam M, Bo Zhang B, McNaughton RL, Kinney RA, Hille R, Brian M, Hoffman BM (2010) The structure of formaldehyde-inhibited xanthine oxidase determined by 35 GHz 2H ENDOR spectroscopy. J Am Chem Soc 132:14015–14017
118. Alfano M, Christine Cavazz C (2018) The biologically mediated water–gas shift reaction: structure, function and biosynthesis of monofunctional [NiFe]-carbon monoxide dehydrogenases. Sustain Energy Fuels 2:1653–1670
119. Spangler NJ, Meyers MR, Gierke KL, Kerby RL, Roberts GP, Ludden PW (1998) Substitution of valine for histidine 265 in carbon monoxide dehydrogenase from *Rhodospirillum rubrum* affects activity and spectroscopic states. J Biol Chem 273:4059–4064
120. Seefeldt LC, Hoffman BM, Dean DR (2009) Mechanism of Mo-dependent nitrogenase. Annu Rev Biochem 78:701–722
121. Solomon EI, Heppner DE, Johnston EM, Ginsbach JW, Cirera J, Qayyum M, Kieber-Emmons MT, Kjaergaard CH, Hadt RG, Tian L (2014) Copper active sites in biology. Chem Rev 114:3659–3853
122. Thorneley RNF, Lowe DJ (1985) Molybdenum Enzymes. Wiley, New York, pp 221–284
123. Lowe DJ, Ashby GA, Brune M, Knights H, Webb MR, Thorneley RNF (1995) Nitrogen Fixation: Fundamentals and Applications. Kluwer, Boston, pp 103–108
124. Seefeldt LC, Yang Z-Y, Lukoyanov DA, Harris DF, Dean DR, Raugei S, Hoffman BM (2020) Reduction of substrates by nitrogenases. Chem Rev 120:5082–5106
125. Rutledge HL, Tezcan FA (2020) Electron transfer in nitrogenase. Chem Rev 120:5158–5193
126. Kang W, Lee CC, Jasniewski AJ, Ribbe MW, Hu Y (2020) Structural evidence for a dynamic metallocofactor during N2 reduction by Mo-nitrogenase. Science 368:1381–1385
127. Bjornsson R, Lima FA, Spatzal T, Weyhermüller T, Glatzel P, Bill E, Einsle O, Neese F, DeBeer S (2014) Identification of a spin-coupled Mo(iii) in the nitrogenase iron–molybdenum cofactor. Chem Sci 5:3096–3103
128. Warmack RA, Rees DC (2025) The nitrogenase mechanism: new roles for the dangler? J Biol Inorg Chem 30:125–133
129. Hoffman BM, Lukoyanov D, Yang ZY, Dean DR, Seefeldt LC (2014) Mechanism of nitrogen fixation by nitrogenase: the next stage. Chem Rev 114:4041–4062
130. Maiti BK, Maia LB, Moro AJ, Lima LC, Cordas CM, Moura I, Moura JJG (2018) Unusual reduction mechanism of copper in cysteine-rich environment. Inorg Chem 57:8078–8088
131. Tian S, Jones SM, Solomon EI (2020) Role of a tyrosine radical in human ceruloplasmin catalysis. ACS Cent Sci 6:1835–1843
132. Munzone A, Eijsink AGH, Berrin J-G, Bissaro B (2024) Expanding the catalytic landscape of metalloenzymes with lytic polysaccharide monooxygenases. Nat Rev Chem 8:106–119